O^1-[6-(METHYLSELANYL)HEXANOYL]GLYCEROL AS AN ANCHOR FOR SELF-ASSEMBLY OF BIOLOGICAL COMPOUNDS AT THE GOLD SURFACE

Bente Jeanette FOSS[a1], Ana ION[b], Vassilia PARTALI[a2], Hans-Richard SLIWKA[a3] and Florinel Gabriel BANICA[a4,*]

[a] *Department of Chemistry, Norwegian University of Science and Technology (NTNU), 7491 Trondheim, Norway; e-mail:* [1] *bente.jeanette.foss@chem.ntnu.no,* [2] *vassilia.partali@chem.ntnu.no,* [3] *hrs@nvg.ntnu.no,* [4] *f.banica@chem.ntnu.no*

[b] *Department of Analytical Chemistry and Instrumental Analysis, University Politehnica of Bucharest, Romania; e-mail: ana_ion@chim.upb.ro*

Received September 8, 2003
Accepted May 7, 2004

Presented at the 36th Heyrovský Discussion on Electrochemistry of Biological Systems and Their Models, Třešť, June 15–19, 2003.

Adsorption of O^1-[6-(methylselanyl)hexanoyl]glycerol (SeOG) on the gold surface was investigated by cyclic voltammetry, phase-sensitive AC voltammetry, electrochemical impedance spectroscopy and piezoelectric microgravimetry. SeOG adsorption results in a stable and compact surface layer with the coverage degree close to unity for an adsorption time of 30 to 80 min and 4.6 mM SeOG acetonitrile solution. Such a layer displays minute defects (pinholes) with the radius of ca. 1–3 μm, separated by 6–50 μm intervals (depending on the adsorption time). The adsorbed compound undergoes anodic desorption in the gold oxide region and also undergoes a cathodic process leading to the removal of the surface layer. Both these processes are similar to those demonstrated by short-chain alkanethiols and have been interpreted as a indication for the conversion of the selena to selenol function as a result of a dissociative adsorption process. Apparently, the main component of the surface layer is O^1-(6-selanylhexanoyl)glycerol that results by the cleavage of the C6–Se bond in SeOG. The two free hydroxy groups in SeOG allow to use it as a bridge for binding other compounds to the gold surface. This possibility was illustrated by building up surface layers of a carotenoid derivative (O^1-(8′-apo-β-apo-caroten-8′-oyl)-O^2-[6-(methylselanyl)hexanoyl]glycerol, **II**) or carotenoid- and phosphocholine-derivatized SeOG (O^1-(8′-apo-β-caroten-8′-oyl)-O^2-[6-(methylselanyl)hexanoyl]-O^3-{[2-(trimethylammonio)ethoxy]phosphoryl}glycerol, **III**). The compound **III** generates a less densely packed layer due to the constraints induced by the phosphocholine substituent. Each of these compounds undergoes anodic reactions that are typical of carotenoids in the adsorbed state. However, the polar and hydrophilic phosphocholine residue in **III** shifts the anodic peak to a less pozitive potential. SeOG allows therefore to tune the molecular environment of a surface attached compound by means of a suitable co-substituent.

Keywords: Carotenoids; Glycerol; Selenides; Self-assembled monolayers; Electrochemistry.

Self-assembly of organic compounds at solid surfaces is a convenient method for preparing surfaces with well defined characteristics[1–4]. A straightforward method for preparing self-assembled monolayer (SAM) consists of chemisorption of thiols or disulfides to metals like gold or silver. Disulfide adsorption results in S–S bond cleavage and the ensuing SAM is identical to that generated by the relevant thiol, with the sulfur head strongly attached to the metal surface. The high degree of organization is the result of two combined effects. First, the metal lattice may provide a suitable template. Second, intramolecular interactions within the surface layer stimulate the formation of an orderly network.

The SAM research represents a very active field with promising applications in various areas such as sensor technology[5–7], electroanalytical chemistry[8,9] and microfabrication[10]. In addition to physical methods of surface investigation, electrochemistry provides techniques for exploring properties of SAMs on metal surface, as demonstrates the comprehensive review by Finklea[11].

Although the investigation of organosulfur self-assembled monolayers has been the subject of many publications, selenium derivatives attracted a limited attention. The interest in organoselenium SAMs was initially stimulated by attempts to overcome problems with sulfur as a functional headgroup[12]. Subsequently, the selenium headgroup became attractive from the viewpoint of the conductance of molecular wires, because it enables higher electronic coupling efficiency compared with sulfur[13–15]. This is in accord with the theoretically derived rule stating that the conductance close to the quantum unit can be obtained with a given molecular structure by increasing the atomic number of the anchoring group[16].

Detailed studies on SAM formation at metal surface by alkaneselenols[12,17,18], aromatic selenols[19–21], aromatic diselenides[22–24] and monoselenides[25–27] are available. Due to the relatively weak interaction between gold and selenium, alkaneselenols form incommensurate structures at the gold surface[12], in contrast to alkanethiols which give rise to commensurate surface structures.

Scanning tunneling microscopy (STM) proved that benzeneselenol forms ordered structure upon chemisorption at a gold surface[19]. In contrast, benzenethiolate cannot form organized structures under similar conditions. This behavior was interpreted as a proof for a stronger Au–Se interaction[19], in accord with further investigations by surface-enhanced Raman spectrometry[20] (SERS).

Diselenides undergo Se–Se bond cleavage during adsorption and the resulting SAM is similar to that generated by analogous selenols in accord with the behavior of disulfides[22–24].

In the case of monoselenide adsorption on the gold surface, the state of the adsorbate seems to depend strongly on the structure of the precursor and the SAM preparation procedure. Thus, selenophene undergoes nondissociative chemisorption under atmospheric vapor deposition, whereas the dissociative mechanism takes place upon ultrahigh vacuum deposition[26]. As a rule, the interaction between chalcogenophene analogues and the gold surface is stronger when the atomic number of chalcogen is higher[26].

On the other hand, the aromatic benzyl phenyl selenide is adsorbed in intact form, as proved by SERS investigations[27]. No relevant data in this respect are yet available for dialkyl selenides, but an STM examination demonstrated that dibutyl selenide forms ordered structures at the gold surface[25].

For comparison, it is interesting to note that organic sulfides preserve the structure when adsorbing on the gold surface[28–36]. Some exceptions are still possible[30]. Thus, an X-ray photoelectron spectrometry (XPS) investigation demonstrates that dioctadecyl sulfide is physically adsorbed from a 1 mM CH_2Cl_2 solution, with no C–S bond cleavage[30a]. However, the C–S bond cleavage seems to occur when a monosulfide SAM was formed during long time immersion at high temperature, or using $CHCl_3$ as a solvent[30a].

We report here the results of an investigation by electrochemical methods and piezoelectric microgravimetry of the adsorption of *O*^{1}-[6-(methylselanyl)hexanoyl]glycerol (SeOG; Table I, formula **I**) on the polycrystalline gold surface. SeOG is a suitable anchor for binding other molecules to the surface via the free hydroxy groups in the glycerol residue. As an example, the binding of a carotenoid (*O*^{1}-(8′-apo-β-apo-caroten-8′-oyl)-*O*^{2}-[6-(methylselanyl)hexanoyl]glycerol; Table I, formula **II**) and both a carotenoid and a phosphocholine fragment (*O*^{1}-(8′-apo-β-caroten-8′-oyl)-*O*^{2}-[6-(methylselanyl)hexanoyl]-*O*^{3}-{[2-(trimethylammonio)ethoxy]phosphoryl}glycerol; Table I, formula **III**) is presented. Carotenoids are of outstanding biological importance, playing a key role in photosynthesis[37]. On the other hand, synthetic supramolecular systems including carotenoids are actively investigated for the purpose of mimicking photosynthetic solar energy conversion[38]. Another stimulus to the study of carotenoids assemblies emerges from the field of molecular electronics, particularly after an evidence of good conductivity of an individual carotenoid molecules has been published[39]. In this context, immobilization of carotenoids to metal surfaces is

an important issue. The thione[40–43], selena[42,44], or thiol function[39,45] has been used to attach carotenoids to the gold surface.

Investigation of SeOG adsorption is an important step before proceeding to the study of the surface behavior of some complex assemblies including SeOG as a bridge. In addition, this investigation allows to acquire more insight into adsorption of organic selenides on the gold surface.

TABLE I
Chemical compounds used as electrode surface modifiers

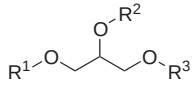

	I	II	III
—R^1	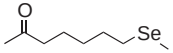	—H	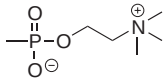
—R^2	—H	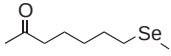	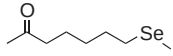
—R^3	—H	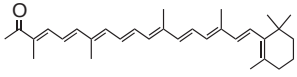	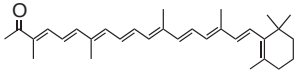

EXPERIMENTAL

SeOG has been synthesized and purified according to the published procedures[46,47]. Compound **II** was synthesized and purified according to the published procedures[48], and **III** was synthesized by an original method[49]. The three compounds have been prepared by specific synthesis, avoiding isomerisation, and have been characterized by common spectroscopic methods (mass spectrometry, nuclear magnetic resonance spectrometry, absorption spectrometry in the visible range). The given structures in Table I are consistent with the spectral data.

Electrolyte solutions were prepared with fresh ultra-pure water (Millipore, resistivity 18 MΩ cm). All the reagents were of analytical grade, except the organic solvents that were of HPLC grade.

A polycrystalline gold disk electrode was prepared from a gold wire (Aldrich 99.99%, 1 mm diameter) sealed by epoxy resin in a glass tube (electrode No. 1). Alternatively, a Metrohm gold disk electrode of 2 mm diameter (electrode No. 2) was used in some experiments. The electrode surface was conditioned by mechanical polishing followed by prolonged cyclic voltammetry scanning in 0.01 M $HClO_4$ in the potential region from 0.00 to 1.45 V. An Ag|AgCl (1 M KCl) reference electrode was connected with the test solution using an 1 M KNO_3 electrolyte bridge; the auxiliary electrode consisted of a platinum plate. Other details are available in[43].

The SeOG adsorption was achieved by immersing the gold substrate in a 4.6 mM SeOG solution in acetonitrile in the dark, at room temperature (20 ± 1 °C), under nitrogen atmosphere. The same procedure was followed with compounds **II** and **III**, except for the composition of the adsorbate solution (4 mM solution of **II** in acetonitrile and 3.9 mM solution of **III** in methanol). After a suitable time period, the electrode was rinsed with the pure solvent and pure water. The modified electrode was then transferred to an aqueous solution containing an appropriate electrolyte, for performing electrochemical investigations.

Staircase cyclic voltammetry (CV), phase-sensitive alternating current voltammetry (ACV) and electrochemical impedance spectroscopy (EIS) experiments have been performed at room temperature (20 ± 1 °C) with Autolab PGSTAT 30 (Eco Chemie). Whenever the electrical charge had to be assessed, CV was run in the "integration" mode, i.e. the output was recorded as the average current over each potential step. Dissolved oxygen was removed from the test solution by bubbling with pure nitrogen. During experiments, nitrogen stream was directed above the solution. The EIS measurements have been performed in 0.1 M KNO_3 containing 5 mM $[Fe(CN)_6]^{3-}$ and $[Fe(CN)_6]^{4-}$ at the equilibrium potential (determined by potentiometry under open circuit conditions) and with a superimposed sine wave voltage of 10 mV.

Fitting and simulation of the electrochemical data was done with Autolab GPES 4.8 and FRA 4.8 software. Additional data reduction operations have been carried out with Origin® 6.1 software (OriginLab Corporation).

An electrochemical quartz crystal microbalance (EQCM) model 5510 (Institute of Physical Chemistry, Warsaw, Poland)[50] was connected to the auxiliary analog input of the PGSTAT 30 instrument to record simultaneously the electrolytic current and the EQCM frequency. A 10 MHz piezoelectric crystal with Ti-backed gold electrodes (5.0 mm diameter) has been mounted in vertical position. The Ti underlayer was selected to prevent problems at extreme anodic potentials[51]. The piezoelectrode had an electrochemically active area of 23.6 mm^2 and a roughness factor of 1.54 (determined according to[52a]). The calibration of the EQCM was performed with the anodic stripping peak of silver[50]. Prior to SeOG adsorption, the piezoelectrode surface was conditioned by three CV scans under the same conditions as with the polycrystalline gold electrodes.

RESULTS AND DISCUSSION

Anodic Behavior of Adsorbed SeOG Layer

An evidence of SeOG adsorption is provided by the anodic behavior of the modified electrode (Fig. 1a). The first scan (curve *1* in Fig. 1a) displays the anodic peak A, which is lower in the second scan (curve *2*). The 3rd and 4th scans are identical and differ very few from the second one. It is clear that a steady state was already attained during the 3rd scan. The above finding demonstrates that SeOG adsorbs irreversibly during the electrode contact with the SeOG solution in acetonitrile. The peak A, which is similar to that induced by a short-chain alkanethiol SAM [11], can be assigned to the oxidative desorption of the organic surface layer. The anodic desorption occurs

almost completely during the first scan, as proved by a comparison of curves *2* and *4* in Fig. 1a. Simultaneously gold oxidation takes place. Gold oxide reduction occurs in the region of the cathodic peak B. Peak B current after desorption (Fig. 1a, curves *2–4*) is higher than that recorded with the clean gold electrode (curve *5*). This trend was detected with all gold electrodes used in this work and point to an increase in the real surface by cor-

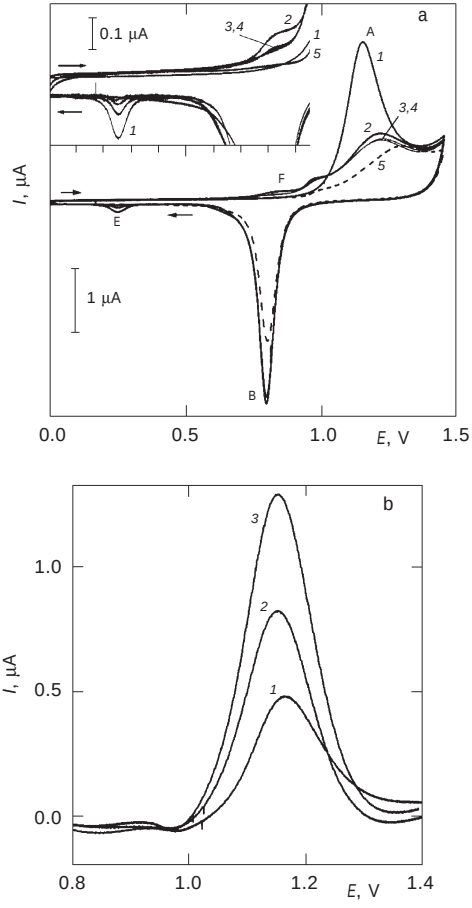

FIG. 1

a Electrochemical behavior of the SeOG-modified gold electrode (No. 1) in the anodic potential region, 0.01 M $HClO_4$. Adsorption time 60 min, scan speed 20 mV s^{-1}. *1* 1st scan; *2–4* subsequent scans; *5* plain gold electrode. Peak A: anodic desorption and gold oxidation; peak B: gold oxide reduction. Inset: enlarged view of the CV curves in the potential region from 0.0 to 0.9 V. b Background corrected voltammograms showing the anodic desorption current in the region of peak A. Adsorption time (in min): *1* 1; *2* 6; *3* 60. For other conditions see Fig. 1a

rosion during the formation of the adsorbed layer. Such a process was investigated in details in connection to adsorption of alkanethiols[52b]. As in that case, the corrosion degree increases with the adsorption time. Thus, the peak B current remained almost unchanged after desorption when the adsorption time was 1 min but increased with this parameter. Moreover, lit.[52b] demonstrates that polar solvents like acetonitrile (which has been used in this work) favor the corrosion. A direct proof for an increase in the real surface during adsorption was provided by the alternating current (AC) capacity recorded (i) at pure gold, before performing the adsorption, and (ii) after performing the anodic desorption as in Fig. 1a. The capacity current was always higher after desorption than before adsorption. On the other hand, Fig. 1a demonstrates that the peak B appears to be unchanged with the advance of the scan sequence. A similar behavior was also noticed with a gold electrode modified with 4′-thioxo-β,β-caroten-4-one[43]. The molecular structure of the adsorbate and its hydrophilic character allows water molecule to approach the metal surface in order to provide the oxygen required in the anodic reaction. Consequently, maximum coverage by oxygen is already attained during the first scan. This contrasts the behavior of alkanethiol SAMs. Due to both compact structure and hydrophobic character, an alkanethiol layer may prevent efficiently the formation of the gold oxide layer.

Figure 1b displays several background subtracted voltammograms for the anodic desorption process. In each case, the background was the gold oxidation current measured on the steady state curve. For six different modification times, ranging from 1 to 60 min, the corrected curve has a symmetrical shape with a peak potential of 1.15 ± 0.01 V and half-width of 0.132 ± 0.006 V. The invariability of the peak parameters proves that the mechanism of the oxidative desorption does not change with the increase in the surface coverage degree. This behavior may be assumed as an evidence of the absence of strong intramolecular interaction in the surface layer.

Selenium Transformations in the Anodic Potential Region

Figure 1a displays the cathodic peak E at 0.25 V on the first reverse scan. This peak should be due to a reaction product of the processes that occurs on the previous anodic scan. The anodic counterpart of E forms at 0.75 V on the next scan (peak F); it is distorted due to the interference of gold oxide formation. An enlarged view of the E/F couple is shown in the inset to Fig. 1a. The inset demonstrates that this couple vanishes after a few scans.

Peaks E and F may be related to electrochemical reactions involving selenium, which was initially present in the adsorbed organic layer. In order to assess their nature, cyclic voltammograms have been recorded for a selenious acid solution in the same background electrolyte (Fig. 2). The first anodic scan (from 0.4 to 1.45 V, curve *1* in Fig. 2) displays only the anodic reaction of gold with minute differences from the curve recorded in the background electrolyte alone (curve *3*). However, the reverse scan displays the cathodic peak E′ at the same potential as the peak E in Fig 1a. On the subsequent anodic scan (curve *2*), the product of peak E′ reaction is oxidized in the region of the peak F′ which lies at the same potential as the peak F in Fig. 1a. It is important to note that the peak E′ appeared even if the previous anodic scan was limited to 0.95 V so as to prevent any anodic reaction.

In agreement with lit.[53a], the peak E′ is ascribed to the reduction of selenite ion adsorptively accumulated at the electrode surface during the previous anodic scan. Se(0) results and is further reoxidized to SeO_3^{2-} in the region of the peak F′. Peak E′ does not form if the first scan starting at 0.4 V goes in the cathodic direction. In this case, SeO_3^{2-} reduction involves bulk solution ions and results in a broad peak with the half peak potential at 0.125 V. The tail of this peak is responsible for the asymmetric shape of the peak E′.

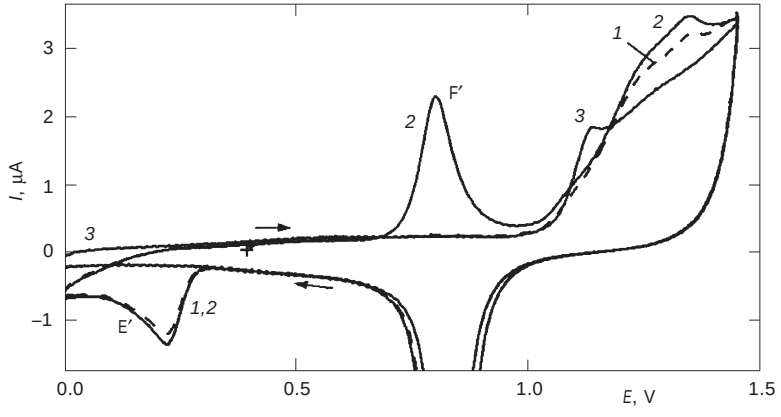

FIG. 2

Two cyclic voltammetric scans in the presence of 50 μM H_2SeO_3 in 0.01 M $HClO_4$ (curves *1* and *2*) and in 0.01 M $HClO_4$ alone (curve *3*). Start at 0.40 V in the anodic direction. Scan speed 20 mV s^{-1}; electrode No. 2

An alternative interpretation[53b] assumes that the peak E′ is due to the reduction of the selenate ion which form by the anodic reaction of selenite. This point of view is at variance with our data that demonstrate the independence of the peak E′ on any preliminary anodic process.

SeO_3^{2-} adsorption in the anodic region is a reversible process. In order to prove this assertion, Se(0) was deposited and then the electrode was subjected to a series of successive CV scans in the background electrolyte alone, from 0 to 0.95 V and back. Under these conditions, peak F′ is well developed on the first anodic scan, but E′ is disproportionately smaller. Both peaks vanished after a few scans. It is clear that adsorbed SeO_3^{2-} which forms under peak F′ diffuses away when the electrode is polarized at less anodic potentials.

By analogy with the behavior of inorganic selenium, peaks E and F in Fig. 1a can be interpreted as follows. The first anodic scan (curve *1* in Fig. 1a) results in the break of the Se–C bond in the adsorbate and Se(–2) is oxidized to adsorbed SeO_3^{2-} by the uptake of 6 electrons per molecule. SeO_3^{2-} is partially desorbed during the following cathodic scan and the remaining adsorbed form is reduced to Se(0) in the region of peak E. Se(0) is then oxidized to SeO_3^{2-} by the peak F reaction. As long as Se is present in the SeO_3^{2-} form, it may diffuse away leading to the gradual disappearance of both peaks E and F.

EQCM Investigation of the Anodic Processes

The anodic desorption process was monitored by EQCM during a multiscan CV run between 0.375 and 1.450 V (Fig. 3). The cathodic limit was selected so as to prevent SeO_3^{2-} (which form under the first anodic scan) from being reoxidized to Se(0). Consequently SeO_3^{2-} may diffuse freely away and does not affect the mass change on the next scans.

Curve *1* in Fig. 3a shows the shift in the resonance frequency during the first scan and displays a positive maximum in the region of peak A. The maximum is the convolution of two processes: desorption of the adlayer and gold surface oxidation. The first process results in a positive frequency shift and the second induces an opposite effect. Curve *2* in Fig. 3a was recorded during the 4th scan and is typical of a plain gold electrode. It is almost indistinguishable of the 2nd and 3rd scans since the desorption goes close to completion under the first anodic scan. The frequency shift on curve *2* results only from gold oxidation and gold oxide reduction. By subtracting curve *2* from curve *1* in Fig. 3a, curve *3* results, which represents the remaining effect of the desorption process only. It is clear from this

curve that the negative mass variation is an effect of an irreversible desorption process that occurs under the direct scan. The horizontal position of the reverse branch of curve *3* demonstrates that no readsorption occurs during the reverse potential sweep. The absence of the readsorption may be due to the oxidative transformation of the Se head into SeO_3^{2-} which at least partially remains in the adsorbed state and may diffuses away during an anodic scan, in accordance with the conclusion of the previous section.

The mass change corresponding to the desorption process was 39.6 ng for a modification time of 17 min (Fig. 3) and of 50.6 ng for a modification time of 30 min. The electrical charge corresponding to the desorption process was of 164 and 188 μC, respectively. Accordingly, 23 and 25.8 g, respectively, correspond to the transfer of 1 mol of electrons.

If we accept that SeO_3^{2-} forms, 6 electrons per molecule are expected to be transferred. A mass-charge correlation leads to 11 electrons per molecule if SeOG was adsorbed in unaltered form and desorbs in the anodic region. If

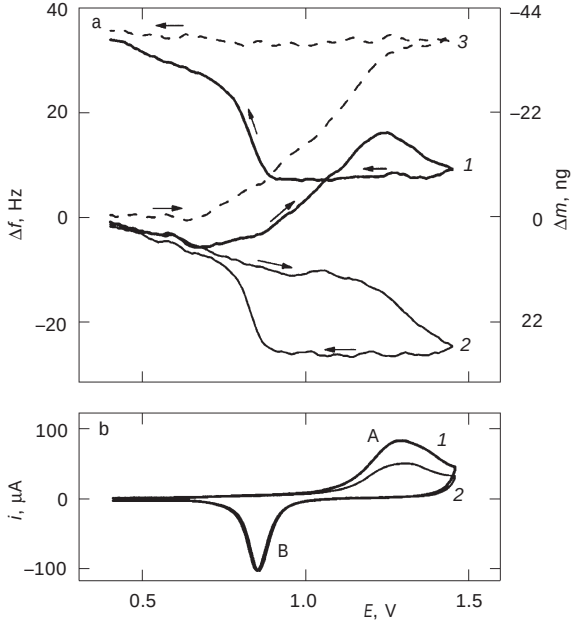

FIG. 3

The EQCM (a) and CV data (b) for the anodic desorption at a SeOG-modified gold piezoelectrode, 0.1 M $HClO_4$. Adsorption time 17 min, scan speed 50 mV s^{-1}. *1* 1st scan; *2* 4th scan; *3* the result of subtracting curve *2* from curve *1* in a

we infer that SeOG splits under adsorption and the product (O^1-(6-selanylhexanoyl)glycerol, SeHG) desorbs, this ratio is 10.4. Both figures are non realistically high. These ones have been calculated under the hypotheses that selenium also leaves the surface during the anodic process of peak A. On the contrary, if it is assumed that SeO_3^{2-} remains in the adsorbed state and only the hydrocarbon fragment is removed, a ratio of about 6 electrons per molecule results, in accordance with the oxidation of Se(–2) to Se(+4). However, the irreversible adsorption of SeO_3^{2-} is a limiting case, which is at variance with the results in the previous section.

It is likely that, in addition to removal of organic adlayer, the shift in frequency is partially determined by other factors, like insertion of water into irregularities of the gold surface. At the same time, SeO_3^{2-} contribution to the mass shift cannot be assessed because it desorbs partially and diffuses away gradually during the first potential scan. On the other hand, the redistribution of electric charges at the interface after removing the organic layer may contribute substantially to the overall current, leading to an overestimation of the charge for the anodic desorption. Data in Fig. 1b also lead to anomalous charge values (1.04 mC per cm^2 of geometric area, for curve *3*). In this case, the high rugosity of the mechanically polished electrode may contribute to the high charge value, in addition to the non-Faradaic process.

It is clear that the complexity of the anodic reaction and the intercourse of Faradaic and non-Faradaic processes prevent a reliable interpretation of the EQCM data. Despite these limitations, data in Fig. 3 demonstrate that the SeOG-generated SAM is relatively stable in the anodic region up to the onset of gold oxide formation.

Kinetics of SeOG Adsorption

The capacity current recorded by ACV (Fig. 4, curve *1*) enabled assessing the changes in the surface state as a function of SeOG adsorption time. The capacity current decreases with the increase in the modification time and becomes almost independent of the electrode potential. This behavior is similar to that demonstrated by alkanethiol SAMs [11]. In terms of the Helmholtz model, this behavior proves that adsorption leads to an increase in thickness of the Helmholtz layer and a decrease in the dielectric constant as a result of water substitution by the organic absorbate. No indication of multilayer formation was noticeable.

The electric charge passed during the anodic desorption allows, in principle, to calculate the amount of adsorbed compound, provided the stoichio-

metry of the electrochemical reaction is exactly known. As far as such information is not yet available, the charge itself may be used as a variable in the adsorption kinetic equation instead of the surface concentration of the adsorbate. This procedure was adopted in this work with some additional precautions. Thus, in order to make sure that the desorption is completed, three successive CV scans as in Fig. 1a have been performed in each case. The total charge (Q_t) for the anodic process occurring from 1.00 to 1.45 V was calculated for each of the three scans. It was assumed that it represents the sum of three components corresponding to adsorbate anodic desorption (Q_d), gold oxide formation (Q_{Au}) and oxygen evolution (Q_{ox}):

$$Q_{t,i} = Q_{d,i} + Q_{Au,i} + Q_{ox,i} \,. \qquad (1)$$

The subscript i stands for the scan number (i = 1–3). As a rule, the desorption is complete after the second scan and the total charge for the third scan ($Q_{t,3}$) results from the contribution of the last two terms in Eq. (*1*). Therefore, the overall charge for the anodic desorption ($Q_d = Q_{d,1} + Q_{d,2}$) was calculated as follows:

$$Q_d = Q_{t,1} + Q_{t,2} - 2Q_{t,3} \,, \qquad (2)$$

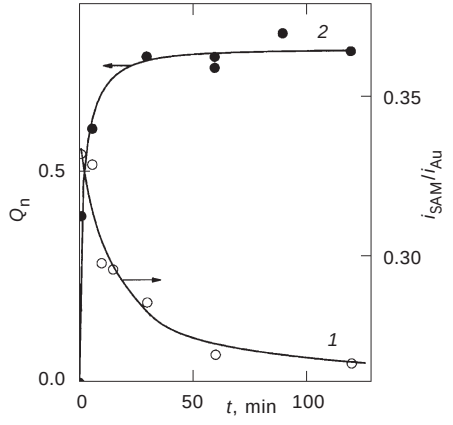

FIG. 4

Effect of the adsorption time on the AC capacity current at 0.00 V (*1*) and on the normalized desorption charge for the anodic desorption under the conditions of Fig. 1a (*2*). Electrode No. 1. Curve *1* conditions: 0.01 M $HClO_4$, frequency 200 Hz, amplitude 5 mV, phase angle –90°. To account for the variability in the surface area, the AC for the covered electrode (i_{SAM}) was normalized to the AC measured after performing the anodic desorption (i_{Au})

where $Q_{t,1}$ and $Q_{t,2}$ denote the total charge for the first and second scan, respectively.

In order to remove the effect of random variations in the electrode surface area, Q_d was normalized to the electric charge for peak B (Fig. 1a). This charge (Q_B) was assumed to be proportional to the real electrode area and was calculated as the average of three succesive scans. Therefore, the normalized desorption charge (Q_n) was calculated as follows:

$$Q_n = Q_d/Q_B \,. \tag{3}$$

With the aim of investigating the kinetics of the adsorption, Q_n was measured after performing the modification for various time intervals, t (Fig. 4, curve *2*) and the Q_n–t curve was checked by various kinetic models. The best fit resulted when using the diffusion-controlled Langmuir kinetic model[54,55], formulated as follows:

$$Q_n = Q_{n,l}[1 - \exp(-K_{DL}ct^{1/2})] \,, \tag{4}$$

where $Q_{n,l}$ is the limiting value of the normalized charge and c stands for the solution concentration of the adsorbing species. The constant K_{DL} depends on the adsorbate diffusion coefficient (D) and surface concentration at equilibrium[54] (Γ_e):

$$K_{DL} = \frac{2}{\Gamma_e}\left(\frac{D}{\pi}\right)^{1/2} \,. \tag{5}$$

The effect of the adsorption time on Q_n is shown in Fig. 4, curve *2*, which demonstrates that Q_n attains a limiting value for adsorption time over 30 min. The limiting specific charge is of 13.6 mC cm^{-2}, in a reasonable agreement with data in Fig. 1b, curve *3*. The difference is a consequence of the variability in the electrode real surface. Under the conditions of Fig. 4, curve *2*, the fitting by Eq. (*4*) results in K_{DL} = 18 l mol^{-1} s$^{-1/2}$ and $Q_{n,l}$ = 0.784. The validity of the diffusion-controlled Langmuir model demonstrates that the adsorption itself is a fast process and the mass transfer of the adsorbate determines the overall rate. This conclusion remains valid despite the approximated character of Eq. (*2*) and is in a fair agreement with curve *1* in Fig. 4.

It is interesting at this point to mention the kinetic features of dialkyl sulfide adsorption on the gold surface[33]. The adsorption rate for such com-

pounds is very low and no diffusion control of the rate-determining step was detected. This behavior strongly contrasts with that of SeOG.

Cathodic Behavior of the SeOG Adsorbed Layer

Cathodic reactions at an organosulfur-SAM-covered electrode allows to distinguish between the thiol or thioether form of the adsorbate. As pointed out before, thioether undergoes physical adsorption with no significant modification in the oxidation state of the gold site. In contrast, thiol adsorption is an oxidative process that was represented as follows[11]:

$$Au_n + HS–R \rightarrow (Au_{n-1}Au^+)^-S–R + 1/2\ H_2\ . \qquad (6)$$

Consequently, a reduction reaction occurs when the SAM covered electrode is polarized to a sufficiently cathodic potential[11]:

$$(Au_{n-1}Au^+)^-S–R + e + H^+ \rightarrow Au_n + HS–R\ . \qquad (7)$$

This reaction is accompanied by desorption. In contrast to thiols, thioethers do not develop a cathodic response[34]. Moreover, thioether layers are destroyed by contact with the aqueous alkaline solution that is used as electrolyte in cathodic desorption experiments[28]. By analogy, a cathodic response of the SeOG-modified electrode may be interpreted as an evidence of the occurrence of the adsorbate in the selenol form.

Figure 5a displays successive CV scans that have been recorded in the potential region from 0 to –1.5 V with a SeOG-modified electrode (the vertex point is out of scale). On the first cathodic scan, three successive peaks, labeled C1, C2 and C3 appeared. Peak C1 vanished after the first scan, whereas C2 and C3 diminished gradually and disappeared after the fourth scan.

The state of the electrode surface after the scans in Fig. 5a was assessed by recording the AC under the conditions of Fig. 4, curve *1* and by probing the anodic behavior under the conditions of Fig. 1a.

The AC increased by a factor of about 3 after performing the CV scans in Fig. 5a and reached a value that was close to that measured for the plain gold electrode. On the other hand, an anodic CV scan following the cathodic polarization does not display any evidence of surface coverage (Fig. 5b, curve *6*). It is clear therefore that the peaks C1–C3 in Fig. 5a arise from a cathodic desorption process similar to that induced by a thiol SAM (reaction (*7*)). This behavior suggests that the C–Se bonds split by adsorption

and the actual adsorbate is a product or a mixture of SeOG molecule cleavage products (i.e. methaneselenol and SeHG).

The fine structure of the cathodic response may be interpreted on the basis of the results of the cathodic desorption of alkanethiol SAMs [56,57]. Accordingly, the fine structure appears due to the desorption of thiolates from domains with different size and organization degrees. Thus, the wave C1 may be assigned to the desorption of small ordered domains or disorganized domains. A comparison of the capacitive current values in Fig. 5a, measured on direct scans in the region between 0 and –0.4 V, shows a marked difference between the first and the second scan, followed by minor changes on the following scans. This implies that most of the adlayer was removed in the C1-wave region, during the first scan. An oxidative readsorption is hardly visible on the reverse branch of CV curve *1* in Fig. 5a (at about –0.7 V) and is missing on the next scans. Consequently, it may be inferred that the surface compound is rapidly lost in the bulk solution, in accord with the fair solubility of SeOG in water. For this reason, waves C2 and C3 cannot be assigned to capacitive processes due to the rearrangement of the desorption products inside the double layer region. These waves may rather be ascribed to the removal of organized domains that require a higher activation energy for desorption. Data in Fig. 5a suggest that ordered

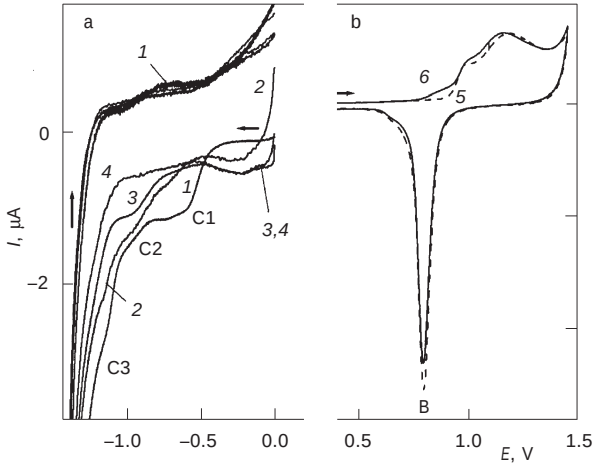

FIG. 5

a Cyclic voltammetry at a SeOG-modified electrode (No. 2) in the cathodic region. *1* 1st scan; *2* 2nd scan; *3* 4th scan; *4* 5th scan. Electrolyte 0.5 M KOH; scan speed 100 mV s^{-1}, modification time 30 min. b CV scans in the anodic region under the conditions of Fig. 1a. *5* Plain gold electrode; *6* the modified electrode, after the experiment in Fig. 5a

domains might form only a minor part of the adlayer, in accord with the heterogeneous crystal structure of the gold substrate.

An alternative interpretation of the fine structure in Fig. 5a may rely on the hypothesis of a mixed adlayer including both methaneselenol and SeHG. However, this interpretation is at variance with the data in Fig. 1b, which demonstrate no fine structure for the anodic desorption signal. The high solubility and mobility of methaneselenol, as well as the competition by SeHG may prevent it from accumulating at the gold surface.

The cathodic reaction of the SeOG-modified electrode was also investigated by EQCM. The voltammogram recorded at the gold piezoelectrode (Fig. 6, curve *1*) shows the same features as those obtained with the electrode 2 (Fig. 5a), i.e. at least three distinct cathodic peaks. For comparison, the potentials of C1–C3 (Fig. 5a) have been indicated by vertical dotted lines in Fig. 6. It is known that electrochemical experiments in alkaline solutions are sensitive to impurities, e.g. oxygen. In order to prove the absence of such problems, the voltammogram *2* in Fig. 6 was recorded at the clean gold electrode. It is clear that no spurious electrochemical reactions occur in the region of peaks C1–C3. Owing to the difference in substrate crystallinity, the height of cathodic peaks in Fig. 6 differs from that in Fig. 5a. The dominant peak in Fig. 6 is C2, previously assigned to the desorption of organized domains. Such domains must be more extended at the surface of an evaporated gold substrate like that used in the EQCM ex-

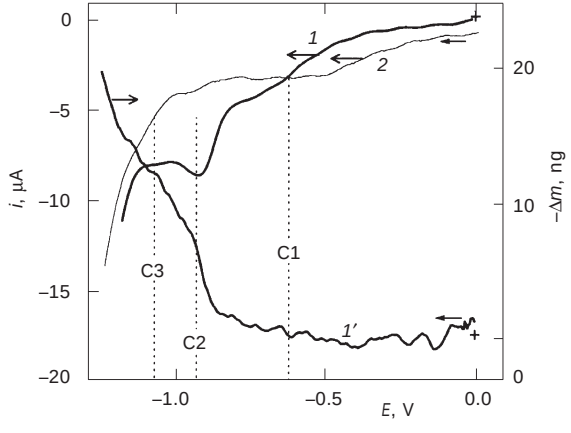

FIG. 6

EQCM data for the cathodic reactions at a SeOG-modified gold piezoelectrode, 0.5 M KOH. Scan speed 50 mV s^{-1}, modification time 17 min. *1* Current–potential curve; *1′* EQCM response; *2* voltammogram recorded at the clean gold surface

periment. In accord with the cathodic peak current, a major shift in the resonance frequency corresponds to the peak C2 (Fig. 6, curve *2*), whereas a minute frequency change accompanies the slight signal C1. The strong increase in Δf at extreme cathodic potentials is probably due to the formation of hydrogen bubbles[58], which prevent the detection of frequency changes associated with C3.

EQCM data confirm that the Faradaic cathodic currents at the SeOG-modified electrode are accompanied by the removal of the adlayer, as it happens in the case of alkanethiol SAMs [56,57,59] when the degree of organization for the SeOG-generated surface layer strongly depends on the crystal structure of the gold substrate. On the other hand, the cathodic behavior of the SeOG-generated layer is similar to that of a benzeneselenol SAM generated by adsorption of diphenyl diselenide[24]. In order to find the correlation between the mass change and the electric charge, peak C2 in Fig. 6 was selected. The electric charge calculated after performing polynomial baseline correction was correlated with the mass change measured by EQCM. The result (266 g/F) demonstrates that the desorbed species is SeHG (molar weight 268) and one electron is consumed per each molecule, in accord with the stoichiometry of alkanethiol desorption (Eq. (*7*)).

Coverage Degree and Surface Layer Morphology

The state of the adsorbed SeOG layer was assessed by assuming that it follows the microdisk array model[11,60,61]. According to this model, the modified surface exhibits non-covered metal islets (pinholes) where the direct contact with the solution phase is possible. Consequently, if a modified metal surface acts as a working electrode in the presence of an electroactive compound, the latter may react at pinhole sites only. It was assumed for simplicity that the pinholes are disk-shaped, have a uniform size (radius r_a) and are separated by constant intervals ($2r_d$).

An analysis of the EIS data for a reversible redox system at an electrode covered by an inert SAM makes it possible to calculate the coverage degree (θ) as well as the parameters[60,61] r_a and r_d. This approach is valid for $1 - \theta < 0.1$, where the following equation holds:

$$1 - \theta = r_a^2 / r_d^2 \quad . \qquad (8)$$

Although the geometry of the pinhole array should be more complex, this model offers an insight into the average pinhole parameters and pro-

vides a basis for the interpretation of experimental conditions effects on the coverage degree and the morphology of the adsorbed layer.

Data from EIS for the $[Fe(CN)_6]^{3-}/[Fe(CN)_6]^{4-}$ couple have been collected for several modification times (Table II). Data passed the Kroning–Kramer test[62] and fit well the Randles circuit including a constant phase element (CPE) instead of a pure capacitor. Here, the impedance of the CPE was defined as follow[63a]:

$$Z_Q = (j\omega Y_0)^{-n}, \qquad (9)$$

where $j = (-1)^{1/2}$, ω is the angular frequency, and Y_0 and n are the parameters of the CPE ($0 < n < 1$). Data in Table II demonstrate that the charge transfer resistance (R_{ct}) increases with the modification time, pointing to a similar variation of the coverage degree. Double-layer capacitance (C)[63b] values are significantly higher for pure gold than for the modified electrode, demonstrating that the hydrophobic polymethylene moiety in SeOG determines the charge distribution at the modified interface. This interpretation is also supported by variation of the n coefficient, which approaches the value for an ideal capacitor ($n = 1$) with increasing modification time. At the same time, the Warburg impedance slope (σ), Eq. 12 is, as expected, almost insensitive to the surface modification. This proves that the mass transport is localized in the solution phase only and the partition of the redox probe between the solution phase and the adsorbed layer (as emphasized in[64]) has no effect in this system. Small fluctuations in the solution resistance (R_s) are due to the uncontrolled changes in the position of the electrolyte bridge tip.

TABLE II
Parameters of the Randles circuit for the SeOG-modified gold electrode with the estimated percent errors in parentheses. The same experimental conditions as in Fig. 7

Modification time, min	R_s Ω cm^2	R_{ct} Ω cm^2	CPE			σ Ω^{-1} s$^{1/2}$ cm^{-2}	C μF cm^{-2}
			Y_0, Ω$^{-1/n}$ s	n	Y_0^n, Ω^{-1} s^n cm^{-2}		
0	5.14(0.41)	2.16(1.93)	$5.54\cdot10^{-7}$(9.8)	0.864(1.72)	$1.25\cdot10^{-4}$(23)	29.1(0.26)	36.8(26.64)
30	2.79(0.85)	42.8(0.46)	$3.92\cdot10^{-8}$(1.23)	0.889(0.36)	$3.32\cdot10^{-5}$(5.57)	29.3(1.15)	14.6(6.04)
80	5.61(0.41)	780.3(0.26)	$3.82\cdot10^{-7}$(1.06)	0.959(0.13)	$2.23\cdot10^{-5}$(2.1)	29.1(2.37)	18.6(2.17)

The Warburg impedance slope, σ, was calculated using the fitting parameter Y_0 for the Warburg impedance as $1/(\sqrt{2}\cdot Y_0)$. C was calculated as $Y_0^n(\omega''_m)^{n-1}$ (ref.[63b]), were ω''_m correspond to the maximum Z'' value in the Z'–Z'' semicircle.

Pinhole parameters have been determined by the method of Finklea et al.[60], which consists of the analysis of the Faradaic impedance (Z_F) dependence on the frequency of the superimposed AC voltage, according to the following relations:

$$Z'_F = \frac{R_{ct}}{1-\theta} + \frac{\sigma}{\omega^{1/2}} + \frac{\sigma}{1-\theta}\left[\frac{\left(\omega^2 + q^2\right)^{1/2} + q}{\omega^2 + q^2}\right]^{1/2} \quad (10)$$

and

$$Z''_F = \frac{\sigma}{\omega^{1/2}} + \frac{\sigma}{1-\theta}\left[\frac{\left(\omega^2 + q^2\right)^{1/2} - q}{\omega^2 + q^2}\right]^{1/2}, \quad (11)$$

where Z'_F and Z''_F represent the in-phase and the out-of-phase components of Z_F, respectively. The amounts σ (Warburg impedance slope), R_{ct} (charge transfer resistance) and q were defined as follows:

$$\sigma = \left(\frac{2}{D}\right)^{1/2} \frac{RT/F}{FAc} \quad (12)$$

$$R_{ct} = \frac{RT/F}{FAc\,k^0} \quad (13)$$

$$q = \frac{D}{0.36 r_a^2}, \quad (14)$$

where D and c represent the diffusion coefficient and the concentration of the redox probe components, respectively, whereas k^0 is the standard rate constant for the charge transfer reaction.

The Faradaic impedance was calculated by subtracting from the overall value the contribution of the non-Faradaic components as determined in the high frequency region. Typical patterns for Z'_F and Z''_F dependence on $\omega^{-1/2}$ are presented in Fig. 7. Further, instead of performing a graphical analysis of each linear portions in the Z'_F vs $\omega^{-1/2}$ plot[60], data have been subjected to a non-linear curve fitting procedure, according to either Eq. (*10*) or Eq. (*11*). R_{ct}, σ, θ and q have been the fitting parameters and $\omega^{-1/2}$ the independent variable. Finally, D was calculated from Eq. (*12*) and introduced into Eq. (*14*) to find r_a; r_d was determined from Eq. (*8*). Curves calculated by Eqs (*10*) and (*11*) using numerical values of the fitting parameters were plotted in Fig. 7; they matched very well the experimental values.

Pinhole parameters are summarized in Table III, where θ values satisfy the condition $1 - \theta < 0.1$, in accord with the constraints of this model. At the same time, the values resulting from the fitting by either Eq. (*10*) or Eq. (*11*) are in a fair agreement, proving the validity of the model for this system.

An inspection of the results in Table III demonstrates that both r_a and r_d increase with increasing modification time, although θ undergoes very slight change. This effect may be interpreted as a result of pinhole coalescence leading to the formation of larger islets located at a larger distance

TABLE III
Coverage degree and pinhole parameters for the SeOG-modified gold electrode

Modification time, min	Fitting variable	Coverage degree	r_a, μm	r_d, μm
30	Z'_F	0.969	1.02	5.85
	Z''_F	0.978	1.10	7.41
80	Z'_F	0.994	3.07	49.16
	Z''_F	0.996	2.88	38.46

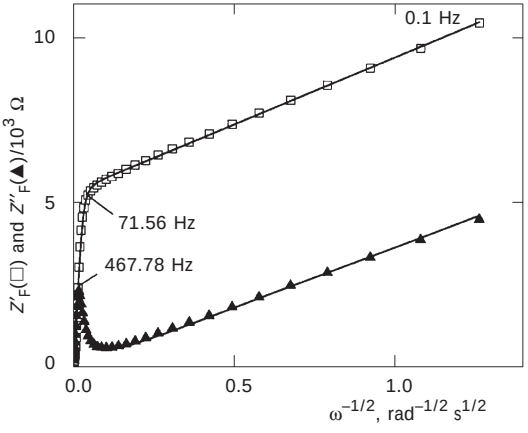

FIG. 7
Faradaic impedances (in-phase Z'_F (□) and out-of-phase Z''_F (▲) components) recorded for the gold electrode (No. 2) modified with SeOG. Adsorption time 30 min. Electrolyte: 0.1 M KNO_3, 5 mM $K_3[Fe(CN)_6]$, 5 mM $K_4[Fe(CN)_6]$. Frequency: from 20 kHz to 0.1 Hz (40 values equally distributed on a logarithmic scale). Lines represent the fitting curves according to Eqs (*10*) and (*11*)

from each other. This demonstrates that the adsorbate molecules experience some mobility, which manifests itself at longer modification times. The coalescence of pinholes was also noticed previously for the dodecane-1-selenol[18] and benzeneselenol[19] surface layers.

The good agreement with the microdisk array model implies that the SeOG-generated SAM fulfils the restrictions of this model[11], namely relatively uniform pinhole dimensions and spacing.

SeOG as an Anchor for Immobilization of Carotenoids at the Gold Surface

We present in this section two examples of SeOG applications in attaching carotenoid derivatives (**II** and **III**) to the electrode surface. For convenience of the synthesis, 6-(methylselanyl)hexanoyl grouping in **II** and **III** was attached as the R^2 substituent in glycerol, in contrast to SeOG where it appears in position 1. Experiments with O^2-[6-(methylselanyl)hexanoyl]glyc-

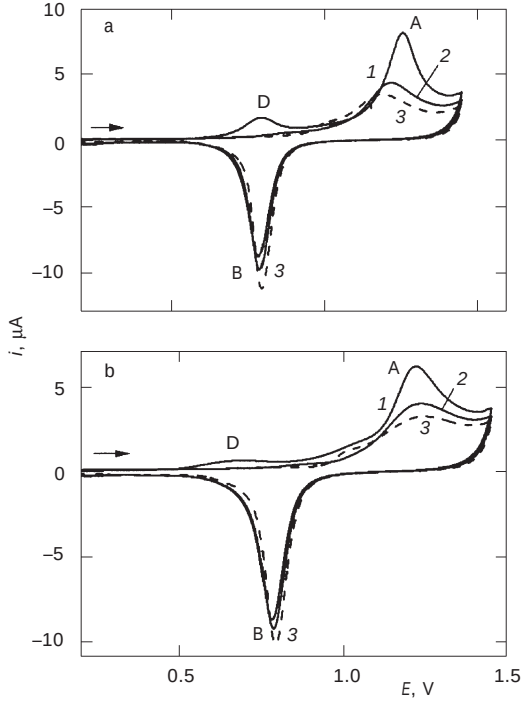

FIG. 8
Anodic reactions at the gold electrode No. 2 modified by compounds **II** (a) and **III** (b). The same conditions as in Fig. 1a. Adsorption time 30 min. *1* 1st scan; *2* 2nd scan; *3* steady state curve

erol in the adsorbed state at the gold surface showed that this behaves similarly to SeOG. Modification of the gold electrode by compounds **II** and **III** was performed by solution phase adsorption, as described in Experimental. The surface was thereafter checked by CV scans in the anodic potential region as in Fig. 1a. As follows from Fig. 8, the presence of each compound at the electrode surface is demonstrated by the anodic desorption peak A, which is similar to that recorded with the SeOG-modified electrode (Fig. 1). This proves that **II** and **III** have been attached to the gold surface through the Se function. Both of them desorb during the first anodic scan (curves *1* in Fig. 8), as the second scan (curves *2*) displays only the anodic wave for gold oxide formation. In both cases, the second scan (curves *2*) is close to the steady state curve (*3*) proving that most of the surface layer was desorbed during the first anodic scan, as it happens with SeOG itself (Fig. 1a). The fact that peak B shows only a minute increases from the first scan to the steady state curve points to the same conclusion.

In addition, both **II** and **III** induce the anodic peak D, which is missing in the case of SeOG (Fig. 1a, curve *1*). An anodic peak like D was previously detected with 4′-thioxo-β,β-caroten-4-one chemisorbed on the gold surface via sulfur[40–43]. Consequently, peak D was assigned to the anodic oxidation of the polyene fragment R^3 (Table I, **II** and **III**), which is a carotenoid residue. In accord with the current view, the first step in such a reaction should be the formation of a cation-radical[65]. In the absence of a nucleophile, this may be further oxidized to a dication. However, in our experiments, the electroactive surface layer is in contact with water that may react immediately with the primary product. Such a process is favored in the case of **III** whose molecule contains the hydrophilic phosphocholine residue. Under these circumstances, the inactivation of the primary product proceeds faster. As a consequence, the peak D for **III** develops at a less positive potential as compared with **II**. At the same time, both peaks A and D are more intensive for **II** (Fig. 8a) than for **III** (Fig. 8b), proving that the phosphocholine substituent constrains the compound **III** adlayer to adopt a less densely packed morphology.

The above results demonstrate that SeOG may act as a convenient bridge for attaching highly-unsaturated compounds like carotenoids to the gold surface. In addition, binding of a second moiety to glycerol allows preparing mixed surface layers. Further details will be reported in a forthcoming paper.

CONCLUSIONS

SeOG interaction with the gold surface leads to the formation of a rather stable and compact adsorbed layer, which shows much of the characteristics of a short-chain alkanethiol SAM. Thus, the adsorbate binds irreversibly to the metal surface and the metal–adsorbate bond has a strongly polar character, as demonstrated by the charge transfer process that accompanies the cathodic desorption. Also, the anodic oxidative reaction reminds of the behavior of adsorbed alkanethiols.

It was demonstrated that SeOG adsorption is accompanied by the cleavage of the C–Se bonds and that the adsorbed layer consists mostly of SeHG. This behavior contrasts with that of dialkyl thioethers, which adsorb in the intact form. The reason for this difference may be the difference in the chemical bond strength for C–S and C–Se (714.1 and 590.4 kJ mol^{-1} at 298 K, respectively), in diatomic molecules[66].

SeOG may act as a convenient bridge for attaching organic compounds to the gold surface through the ester function as evidenced in this paper for carotenoid and phosphocholine derivatives. Further applications of SeOG as an anchor for amine derivatives (including amino acids, peptides and proteins) may be envisaged. In such case, cyanogen bromide or cyanuric chloride would be suitable coupling agents[67].

SYMBOLS

A	area of the electrode surface
c	concentration
C	capacitance
D	diffusion coefficient
f	frequency
F	Faraday constant
k^0	standard rate constant for the charge transfer reaction
K_{DL}	constant in the diffusion-controlled Langmuir model (Eq. (*5*))
n	the exponent of the CPE ($0 < n < 1$)
$Q_{t,i}$	total charge for the peak A on the i-th scan
$Q_{d,i}$	charge for the anodic desorption on the i-th scan
$Q_{Au,i}$	charge for gold oxide formation on the i-th scan
$Q_{ox,i}$	charge for oxygen evolution plus contributions by the double layer modifications on i-th scan
Q_B	charge for the peak B
Q_d	total charge for anodic desorption
Q_n	normalized desorption charge (Eq. (*3*))
$Q_{n,l}$	the limiting value of the normalized charge
r_a	average radius of disk-shaped pinholes
r_d	average half-distance between pinholes

R	gas constant
R_{ct}	charge transfer resistance
R_s	ohmic resistance of the solution
t	time
T	temperature
Y_0	the ideal capacitance
Z_F	Faradaic impedance
Z_F'	the in-phase component of Z_F
Z_F''	the out-of-phase component of Z_F
Z_Q	impedance of the constant phase element
Δf	frequency shift
Γ_e	surface concentration at equilibrium
θ	coverage degree
ω	angular frequency
σ	slope of the Warburg impedance

A. Ion gratefully acknowledges financial support of the Norwegian Research Council.

REFERENCES

1. Ulman A.: *MRS Bull.* **1995**, *20*, 46.
2. Ulman A.: *Chem. Rev.* **1996**, *96*, 1533.
3. Xu J., Li H. L.: *J. Colloid Interface Sci.* **1995**, *176*, 138.
4. Schreiber F.: *Prog. Surf. Sci.* **2000**, *65*, 151.
5. Wink T., van Zuilen S. J., Bult A., van Bennekom W. P.: *Analyst* **1997**, *122*, 43R.
6. Flink S., van Veggel F. C. J. M., Reinhoudt D. N.: *Adv. Mater.* **2000**, *12*, 1315.
7. Gooding J. J., Mearns F., Yang W. R., Liu J.: *Electroanalysis (N. Y.)* **2003**, *15*, 81.
8. Mandler D., Turyan I.: *Electroanalysis (N. Y.)* **1996**, *8*, 207.
9. Mirsky V. M.: *Trends Anal. Chem.* **2002**, *21*, 439.
10. Kumar A., Abbott N. L., Kim E., Biebuyck H. A., Whitesides G. M.: *Acc. Chem. Res.* **1995**, *28*, 219.
11. Finklea H. O. in: *Electroanalytical Chemistry* (A. J. Bard and I. Rubinstein, Eds), Vol. 19, p. 109. M. Dekker, New York 1996.
12. Samant M. G., Brown C. A., Gordon J. G.: *Langmuir* **1992**, *8*, 1615.
13. Patrone L., Palacin S., Bourgoin J. P.: *Appl. Surf. Sci.* **2003**, *212*, 446.
14. Patrone L., Palacin S., Bourgoin J. P., Lagoute J., Zambelli T., Gauthier S.: *Chem. Phys.* **2002**, *281*, 325.
15. Yaliraki S. N., Kemp M., Ratner M. A.: *J. Am. Chem. Soc.* **1999**, *121*, 3428.
16. Di Ventra M., Lang D. N.: *Phys. Rev. B: Condens. Mater.* **2002**, *65*, 5402.
17. Nakano K., Sato T., Tazaki M., Takagi M.: *Langmuir* **2000**, *16*, 2225.
18. Protsailo L. V., Fawcett W. R., Russell D., Meyer R. L.: *Langmuir* **2002**, *18*, 9342.
19. Dishner M. H., Hemminger J. C., Feher F. J.: *Langmuir* **1997**, *13*, 4788.
20. Huang F. K., Horton R. C., Myles D. C., Garrell R. L.: *Langmuir* **1998**, *14*, 4802.
21. Han S. W., Lee S. J., Kim K.: *Langmuir* **2001**, *17*, 6981.
22. Bandyopadhyay K., Vijayamohanan K.: *Langmuir* **1998**, *14*, 625.

23. Bandyopadhyay K., Vijayamohanan K., Venkataramanan M., Pradeep T.: *Langmuir* **1999**, *15*, 5314.
24. Aslam M., Bandyopadhyay K., Vijayamohanan K., Lakshminarayanan V.: *J. Colloid Interface Sci.* **2001**, *234*, 410.
25. Nakamura T., Kimura R., Matsui F., Kondoh H., Ohta T., Sakai H., Abe M., Matsumoto M.: *Langmuir* **2000**, *16*, 4213.
26. Kondoh H., Nakai I., Nambu A., Ohta T., Nakamura T., Kimura R., Matsumoto M.: *Chem. Phys. Lett.* **2001**, *350*, 466.
27. Han S. W., Kim K.: *J. Colloid Interface Sci.* **2001**, *240*, 492.
28. Troughton E. B., Bain C. D., Whitesides G. M., Nuzzo R. G., Allara D. L., Porter M. D.: *Langmuir* **1988**, *4*, 365.
29. Hagenhoff B., Benninghoven A., Spinke J., Liley M., Knoll W.: *Langmuir* **1993**, *9*, 1622.
30. a) Takiguchi H., Sato K., Ishida T., Abe K., Yase K., Tamada K.: *Langmuir* **2000**, *16*, 1703; b) Noh J., Kato S. H., Kawai M., Hara M.: *J. Phys. Chem. B* **2002**, *106*, 13268.
31. Beulen M. W. J., Huisman B.-H., van der Heijden P. A., van Veggel F. C. J. M., Simons M. G., Biemond E. M. E. F., de Lange P. J., Reinhoudt D. N.: *Langmuir* **1996**, *12*, 6170.
32. Lee H. Y., He Z. L., Hussey C. L., Mattern D. L.: *Chem. Mater.* **1998**, *10*, 4148.
33. Jung C., Dannenberger O., Xu Y., Buck M., Grunze M.: *Langmuir* **1998**, *14*, 1103.
34. Zhong C. J., Brush R. C., Anderegg J., Porter M. D.: *Langmuir* **1999**, *15*, 518.
35. Dishner M. H., Hemminger J. C., Feher F. J.: *Langmuir* **1996**, *12*, 6176.
36. Trevor J. L., Lykke K. R., Pellin M. J., Hanley L.: *Langmuir* **1998**, *14*, 1664.
37. Blankenship R. E.: *Molecular Mechanisms of Photosynthesis*. Blackwell, Oxford 2002.
38. Gust D., Moore T. A., Moore A. L.: *Acc. Chem. Res.* **2001**, *34*, 40.
39. Leatherman G., Durantini E. N., Gust D., Moore T. A., Moore A. L., Stone S., Zhou Z., Rez P., Liu Y. Z., Lindsay S. M.: *J. Phys. Chem. B* **1999**, *103*, 4006.
40. Ion A., Banica F. G., Partali V., Sliwka H. R.: *J. Heyrovsky Memorial Symposium on Advances in Polarography and Related Methods, Prague, August 30–September 1, 2000*, Book of Abstracts, p. 63.
41. Ion A., Banica F. G., Partali V., Sliwka H. R.: *International Symposium on New Directions in Electroanalysis, University of Salford, April 22–25, 2001*, Book of Abstracts, Lecture No. 7.
42. Ion A., Banica F. G., Foss, B. J., Partali V., Sliwka H. R.: *13th International Carotenoid Symposium, Honolulu, January 6–11, 2002*, Book of Abstracts, p. 19.
43. Ion A., Partali V., Sliwka H. R., Banica F. G.: *Electrochem. Commun.* **2002**, *4*, 674.
44. Ion A., Banica F. G., Foss, B. J., Partali V., Sliwka H. R.: *13th International Carotenoid Symposium, Honolulu, January 6–11, 2002*, Book of Abstracts, p. 114.
45. Liu D. Z., Szulczewski G. J., Kispert L. D., Primak A., Moore T. A., Moore A. L., Gust D.: *J. Phys. Chem. B* **2002**, *106*, 2933.
46. Kodali D. R.: *J. Lipid Res.* **1987**, *28*, 464.
47. Oghi T., Kondo T., Goto T.: *Tetrahedron Lett.* **1977**, *46*, 4051.
48. Naalsund T., Malterud K. E., Partali V., Sliwka H. R.: *Chem. Phys. Lipids* **2001**, *112*, 59.
49. Foss B. J., Partali V., Sliwka H. R.: Unpublished results.
50. Koh W., Kutner W., Jones M. T., Kadish K. M.: *Electroanalysis (N. Y.)* **1993**, *5*, 209.
51. Hoogvliet J. C., van Bennekom W. P.: *Electrochim. Acta* **2001**, *47*, 599.
52. a) Tian M., Pell W. G., Conway B. E.: *Electrochim. Acta* **2003**, *48*, 2675; b) Edinger K., Grunze M., Woll C.: *Ber. Bunsen–Ges. Phys. Chem.* **1997**, *101*, 1811.
53. a) Andrews R. W., Johnson D. C.: *Anal. Chem.* **1975**, *47*, 294; b) Alanyalioglu M., Demir U., Shannon C.: *J. Electroanal. Chem.* **2004**, *561*, 21.

54. Rahn J. R., Hallock R. B.: *Langmuir* **1995**, *11*, 650.
55. Dannenberger O., Buck M., Grunze M.: *J. Phys. Chem. B* **1999**, *103*, 2202.
56. Wong S. S., Porter M. D.: *J. Electroanal. Chem.* **2000**, *485*, 135.
57. Kawaguchi T., Yasuda H., Shimazu K., Porter M. D.: *Langmuir* **2000**, *16*, 9830.
58. Buttry D. A., Ward M. D.: *Chem. Rev.* **1992**, *92*, 1355.
59. Schneider T. W., Buttry D. A.: *J. Am. Chem. Soc.* **1983**, *115*, 12391.
60. Finklea H. O., Snider D. A., Fedyk J.: *Langmuir* **1993**, *9*, 3660.
61. Amatore C., Saveant J. M., Tessier D.: *J. Electroanal. Chem.* **1983**, *147*, 39.
62. Bonanos N., Steele B. C. H., Butler E. P., Johnson W. B., Worell W. L., MacDonald D. D., McKubre M. C. H. in: *Impedance Spectroscopy* (J. R. Macdonald, Ed.), p. 191. J. Wiley, New York 1987.
63. a) *Autolab Electrochemical Systems*, Application Note Appl0/3 (www.ecochemie.nl); b) Hsu H. C., Mansfeld F.: *Corrosion* **2001**, *57*, 747.
64. Markovich I., Mandler D.: *J. Electroanal. Chem.* **2000**, *484*, 194.
65. Liu D. Z., Gao Y. L., Kispert L. D.: *J. Electroanal. Chem.* **2000**, *488*, 140.
66. Lide D. R. (Ed): *CRC Handbook of Chemistry and Physics*. CRC Press, Boca Raton 2002.
67. Barker S. A. in: *Biosensors, Fundamentals and Applications* (A. P. F. Turner, I. Karube and G. S. Wilson, Eds), p. 85. Oxford University Press, Oxford 1987.